Sociedad Española de Nefrología

nefrología
Revista de la Sociedad Española de Nefrología
www.revistanefrologia.com

Original article

Dysregulation of ferroptosis may participate in the mitigating effect of $CoCl_2$ on contrast-induced nephropathy

Huilin Li[a,*,1], *Shuang Liu*[a,1], *Dan Zhang*[a,1], *Xue Zong*[a], *Gengru Jiang*[a], *Chun Zhu*[b,**]

[a] *Division of Nephrology, Department of Internal Medicine, Xinhua Hospital Affiliated to Shanghai Jiao Tong University School of Medicine, Shanghai 200092, China*
[b] *Department of Nephrology, Chongming Hospital Affiliated to Shanghai University of Medicine and Health Sciences, Chongming Branch, Shanghai 202150, China*

ARTICLE INFO

Article history:
Received 4 August 2022
Accepted 27 August 2023

Keywords:
Contrast-induced nephropathy
$CoCl_2$
TMT
HK-2 cell
Hp
Ferroptosis

ABSTRACT

Background: Contrast agents can directly or indirectly induce renal tubular ischemia and hypoxic damage. Given that cobalt chloride ($CoCl_2$) can protect renal tubules, the protective effect and potential mechanism of action of $CoCl_2$ on contrast-induced nephropathy (CIN) warrant investigation.

Methods: A CIN mouse model was established to determine the protective effect of $CoCl_2$ on renal injury *in vivo*. Then, TMT-based proteomics was performed to determine the differentially expressed proteins (DEPs), following which, enrichment analyses of gene ontology and the KEGG pathway were performed. *In vitro*, a CIN model was constructed with renal tubular epithelial cells (HK-2) to determine the effect of $CoCl_2$ on potential targets and the role of the key protein identified from the *in vivo* experiments.

Results: $CoCl_2$ treatment decreased the levels of BUN and serum creatinine (sCr), while increasing the levels of urea and creatinine (Cr) in the urine of mice after CIN injury. Damage to the renal tubules in the $CoCl_2$ treatment group was significantly less than in the CIN model group. We identified 79 DEPs after treating the *in vivo* model with $CoCl_2$, and frequently observed ferroptosis-related GO and KEGG pathway terms. Of these, Hp (haptoglobin) was selected and found to have a strong renoprotective effect, even though its expression level in kidney tissue decreased after $CoCl_2$ treatment. In HK-2 cells, overexpression of Hp reduced the ferroptosis caused by erastin, while knocking down Hp negated the attenuation effect of $CoCl_2$ on HK-2 cell ferroptosis.

Conclusion: $CoCl_2$ attenuated kidney damage in the CIN model, and this effect was associated with the decrease in ferroptosis mediated by Hp.

* *Corresponding author.*
** *Co-corresponding author.*
E-mail addresses: lihuilin@xinhuamed.com.cn (H. Li), zhuchun26@qq.com (C. Zhu).
[1] Equal contributors, they are co-first authors.
http://dx.doi.org/10.1016/j.nefroe.2024.04.003

La desregulación de ferroptosis puede participar en el efecto mitigador de $CoCl_2$ en la nefropatía inducida por contraste

Palabras clave:
Nefropatía inducida por contraste
$CoCl_2$
TMT
Célula HK-2
Hp
Ferroptosis

RESUMEN

Antecedentes: Los agentes de contraste pueden inducir isquemia tubular renal y daño hipóxico de manera directa o indirecta. Dado que el cloruro de cobalto ($CoCl_2$) puede proteger los túbulos renales, el efecto protector y el mecanismo de acción potencial de $CoCl_2$ en la nefropatía inducida por contraste (NIC) merecen ser investigados.

Métodos: Se estableció un modelo de NIC en ratones para determinar el efecto protector de $CoCl_2$ en la nefropatía *in vivo*. Seguidamente, se realizó un análisis proteómico por TMT para determinar las proteínas diferencialmente expresadas (DEP) y, a continuación, un análisis de enriquecimiento de ontología genética y vía KEGG. *In vitro*, se construyó un modelo NIC en células epiteliales de túbulos renales (HK-2) para determinar el efecto de $CoCl_2$ en los objetivos potenciales y el rol de la proteína clave identificada en los experimentos *in vivo*.

Resultados: El tratamiento con $CoCl_2$ redujo los niveles de BUN y de creatinina sérica e incrementó, a la vez, los de urea y creatinina en la orina de los ratones, tras la lesión NIC. El daño a los túbulos renales en el grupo de tratamiento con $CoCl_2$ fue significativamente menor que en el grupo de modelo NIC. Identificamos 79 DEP tras el tratamiento en el modelo *in vivo* con $CoCl_2$ y observamos con frecuencia ontología genética relacionada con ferroptosis y términos de vías KEGG. De ellos, se seleccionó la haptoglobina (Hp) y se encontró que tenía un fuerte efecto renoprotector, aun cuando su nivel de expresión en el tejido renal se redujo tras el tratamiento con $CoCl_2$. En las células HK-2, la sobreexpresión de Hp redujo la ferroptosis causada por erastina, a pesar de que el descenso de Hp negó el efecto atenuador de $CoCl_2$ en la ferroptosis de las células HK-2.

Conclusión: El $CoCl_2$ atenuó el daño renal en el modelo NIC y se asoció este efecto al descenso de ferroptosis mediada por Hp.

Introduction

The number of patients with cardiovascular and chronic kidney diseases has increased, partly due to a rise in the elderly population. Consequently, there has been an uptick in the use of contrast agents for clinical diagnosis and treatment. A study showed that contrast-induced nephropathy (CIN) is a leading cause of acute kidney injury in hospitalized patients.[1] CIN is characterized by an increase in serum creatinine levels of ≥0.5 mg/dL (≥44 μmol/L) or by ≥25% from the baseline value within 48 h of contrast medium (CM) exposure, provided other causes of acute kidney injury are excluded.[2] Risk factors for CIN encompass renal insufficiency and other clinical risk factors, such as advanced age, a low body mass index (BMI), myocardial infarction, cardiac insufficiency, inflammation, anemia, and bleeding.[3] CIN prolongs hospital stays and increases patient mortality. Various risk factors can contribute to a high incidence of CIN among patients.[4] The pathogenesis of CIN is multifaceted, with contributors, including the high osmotic pressure and viscosity of the CM, intrarenal hemodynamic disruptions, oxidative stress, and inflammatory reactions.[5–7] Direct toxic effects of the CM on vascular endothelial cells, like apoptosis, a surge in intracellular calcium ion concentrations, and DNA fragmentation triggered by ROS, also significantly damage renal tubules.[8]

In the absence of detailed knowledge about the mechanisms at play, no definitive CIN treatment exists. Preventative measures, such as hydration therapy and drug prophylaxis, are routinely applied clinically to mitigate CIN incidence. Sodium bicarbonate hydration, normal saline hydration, and a combination of the two are prevalent hydration therapies. These hydration techniques can enhance blood flow, hastening CM excretion and thus diminishing its toxic impact on renal tubules.[9] Nicorandil can curtail ROS accumulation in mitochondria, amplify renal tubular blood flow, and shield the kidneys from ischemic damage post-CM administration.[10] Hypoxic preconditioning can heighten cell adaptability to hypoxic stress, considerably diminishing or even sidestepping the cell damage inflicted by hypoxia.[11] Based on this insight, one study employed cobalt chloride ($CoCl_2$) as a HIF-1α activator in a subtotal nephrectomy mouse model and discovered that this treatment reduced apoptosis in renal tubular cells, elevated renal tubular cell proliferation, and spurred angiogenesis.[12] Another investigation revealed that treating HK-2 cells with $CoCl_2$ tempered cell inflammation and curbed ROS buildup, thereby safeguarding the renal tubules.[13] It remains to be ascertained whether $CoCl_2$ can alleviate ischemic renal damage instigated by CIN and guard renal tubular cells. It is also crucial to probe the molecular and functional mechanisms steering this potential effect.

To discern the effects and the mechanism of action of $CoCl_2$ on CIN, we devised a CIN mouse model. Post-$CoCl_2$ administration, we gauged renal function indicators, conducted H&E staining to evaluate renal tubular harm, and executed immunofluorescence tests to gauge cell death rates

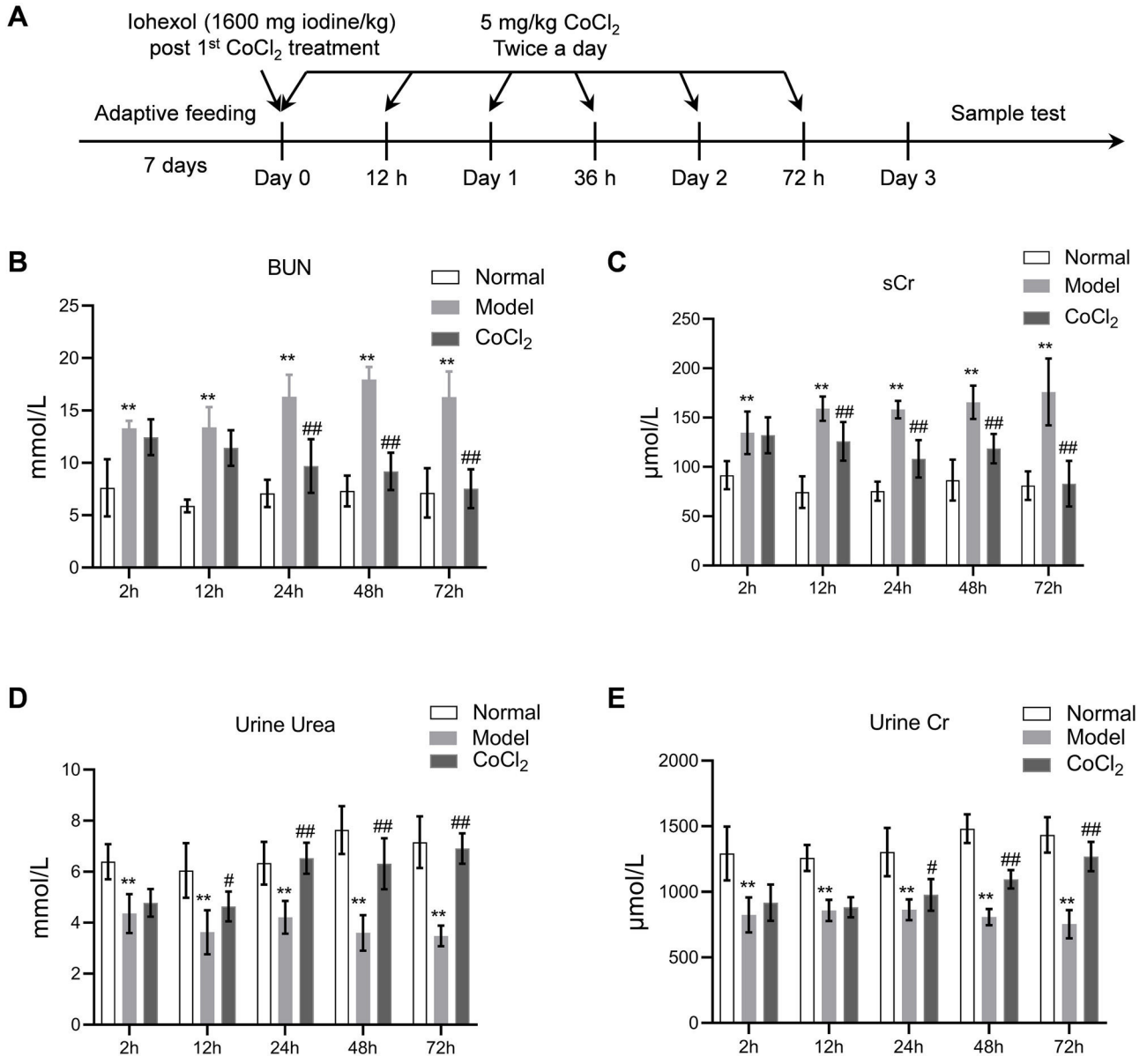

Fig. 1 – Time points in the animal experiment and kidney injury indicators. (A) Time points and experimental procedure. (B–E) Serum blood urea nitrogen (BUN), serum creatinine (sCr), urinary urea, and urinary creatinine after $CoCl_2$ administration; * indicates model *vs.* normal, # indicates $CoCl_2$ *vs.* model; $n = 6$; # $p < 0.05$; **,## $p < 0.01$.

in the renal epithelia. Subsequently, we pinpointed key target proteins using quantitative proteomics and bioinformatics tools. Both Western blotting and qPCR analyses were deployed to confirm the TMT findings. We also formulated an erastin injury model alongside a CIN HK-2 model to elucidate the interplay between the target protein and the renal protection proffered by $CoCl_2$.

Materials and methods

Animals and treatments

Male BALB/c mice (3–4 weeks old) were purchased from Slack Laboratory Animal Co., Ltd. (Shanghai, China). All mice were housed at 22 °C with 30% relative humidity under a 12-h/12-h light/dark cycle and were provided with food and water *ad libitum*. The experiment was approved and supervised by the Animal Protection and Use Agency Committee of Xinhua Hospital Affiliated to Shanghai Jiao Tong University School of Medicine (approval number: XHEC-F-2021-069). All animal procedures adhered to the Laboratory Animal Guidelines for Ethical Review of Animal Welfare (GB/T 35892-2018). After a one-week adaptive feeding period, the mice were randomly divided into three groups ($n = 10$ per group): the normal group, the CIN model group, and the $CoCl_2$ treatment group. A model of contrast-induced nephropathy (CIN) was established using the method described in another study.[14] Briefly, CIN was induced *via* the tail vein. As depicted in Fig. 1A, the administered drug was a hypotonic non-ionic contrast agent (iohexol)

at a single dose of 1600 mg iodine/kg, following the first injection of $CoCl_2$ hexahydrate (Sigma, St. Louis, MO, USA), which was dissolved in distilled water and injected subcutaneously twice a day at a dose of 5 mg/kg. The interval between $CoCl_2$ administrations was 12 h, and each group was treated for 72 h. After each $CoCl_2$ treatment, blood, urine, and kidney tissue samples were collected from each group of mice for analysis.

Enzyme-linked immunosorbent assay (ELISA)

ELISA test kits were utilized to assess the level of kidney injury indicators expression, which included blood urea nitrogen (BUN, ab83362, Abcam), serum creatinine (sCr, ab65340), urinary urea (ab93362), and urinary creatinine (ab65340). The ELISA plates were refrigerated overnight. To generate a standard curve, 100 μL of the appropriate standard was mixed with 100 μL of assay buffer in an ELISA plate well. After mixing, 100 μL of the solution was transferred from one well to the next, repeated five times. Then, 90 μL of assay buffer and 10 μL of the diluted sample were added to the testing well. Next, 50 μL of the diluted antibody solution was added to the corresponding wells. The plates were sealed and shaken for 3 h. The blocking solution was discarded, and 400 μL of wash buffer was added to each well. After a 1-min wash, the washing solution was removed, and this step was repeated four times. Subsequently, 100 μL of the substrate solution was added to each detection well and incubated at room temperature for 15 min. A stop reaction solution (100 μL) was added to end the reaction, changing the color from blue to yellow. The OD value of each well's sample was measured at 450 nm using a microplate reader. The concentration of the detection index for each sample was calculated based on the standard curve.

Hematoxylin and eosin (H&E) staining and PAS (periodic acid-Schiff) staining

Initially, kidney tissue samples were fixed in 4% paraformaldehyde, embedded in paraffin, and sectioned into 5 μm slices. The sections were deparaffinized and rehydrated through a gradient series of xylene and alcohol. They were stained with Harris' hematoxylin solution for 3–8 min and rinsed with double-distilled water, followed by eosin solution staining for 1–3 min. The sections were then dehydrated through a gradient series of alcohols and xylene, dried, and sealed with neutral gum. Under a microscope, these sections were evaluated, and representative images were captured and analyzed. The sections also underwent PAS staining using standard protocols. Once stained, sections were observed under a light microscope, and kidney injuries were assessed and scored based on the proportion of cortical tubular necrosis: 0 = normal, 1 = 1–10%, 2 = 11–25%, 3 = 26–45%, 4 = 46–75%, and 5 = 76–100%.[15] The scoring was conducted in a blinded manner, and nine representative views were used for each sample (three biological replicates were taken from each group).

Proteomics

Kidney tissue samples from each group were pulverized into powder in liquid nitrogen. Proteins were subsequently extracted using the SDT lysis method, comprising 4% (w/v) SDS, 100 mM Tris/HCl pH 7.6, and 0.1 M DTT. The BCA kit facilitated protein quantification. An adequate quantity of protein from each sample was trypsinized *via* the filter-aided proteome preparation (FASP) method. Lyophilized peptides were redissolved in a dissolution buffer (40 μL) and quantified (OD280). For each group, 100 μg of peptides were labeled with a tandem mass tag (TMT) using a commercial kit from Thermo Fisher (Waltham, USA). Once labeled peptides from all groups were combined, they were categorized using AKTA Purifier 100. The Easy nLC HPLC liquid system, operating at a nanoliter flow rate, further separated each fraction. Post-chromatographic separation, the Q-Exactive system (Thermo Fisher) was deployed for mass spectrometry analysis of samples. In primary mass spectrometry, the same peptide segment in different samples labeled with any TMT reagent displays an identical mass-to-charge ratio. In secondary mass spectrometry, the cleavable bond breaks, releasing the TMT reporter ion, producing 10 TMT reporter ion peaks in the mass spectrometer's low mass region. These intensities represent the relative expression of the peptide across different samples. Proteome Discoverer 1.4 16 facilitated protein identification and quantitative analysis.[16] Proteins with an average ratio change of $\geq$1.2 or <0.83, and a *p*-value less than 0.05 were flagged as differentially expressed proteins (DEPs). A hierarchical clustering algorithm organized the differentially expressed proteins, and data was illustrated as a heatmap.

Bioinformatics analysis

Omicsbean (http://www.omicsbean.cn/) annotated the suite of target proteins. This annotation included sequence alignment (Blast), GO entry extraction (Mapping), GO annotation (Annotation), and InterProScan supplementary annotation (Annotation Augmentation). DAVID Bioinformatics Resources v6.8 (https://david.ncifcrf.gov/) conducted the Kyoto Encyclopedia of Genes and Genomes (KEGG) pathway analysis. Using the STRING (http://string-db.org/) database, both direct and indirect interactions among target proteins were discerned and visualized *via* Cytoscape, facilitating an interaction network analysis.

Cell culture and treatment

Human kidney 2 (HK-2) cells were procured from the Cell Resource Center of the Institute of Basic Medicine, Chinese Academy of Medical Sciences. HK-2 cells thrived in DMEM enriched with 10% FBS, 100 U/mL penicillin, and 100 μg/mL streptomycin in a 37 °C incubator. Cells were treated according to the requirements of the experimental groups. The normal group underwent routine cultivation. The model group received a supplement of 100 mg/mL serum-free medium containing iohexol, and its osmotic pressure was fine-tuned to 424 mOsm/L, establishing an *in vitro* model of contrast-induced acute kidney injury (CI-AKI). Stemming from the model group, the $CoCl_2$ group received a 150 μM $CoCl_2$ dose. The *Hp* knockdown and Hp-overexpression groups were exposed to respective viral vectors for cell transfection. Upon treatment completion, cells were harvested for subsequent experiments.

Transfection

The Hp shRNA, manufactured by GenePharm (Shanghai, China), was cloned into the pShuttle-H1 adenovirus plasmids. Additionally, the Hp coding sequence was synthesized and inserted into pShuttle-CMV adenovirus shuttle plasmids (Agilent, Beijing, China). Following the co-transfection of the blank pAdEasy-1 adenovirus skeleton plasmid (Addgene Headquarters, Watertown, MA, USA) with either pShuttle-H1-sh-Hp or pShuttle-CMV-Hp into HEK 293T cells using Lipofectamine 2000 (Invitrogen), a high-titer adenovirus vector was produced. After transfection, adenovirus plasmids generated through recombination were collected after 48 h and then introduced into HK-2 cells. Negative controls were established using cells that were transduced with either the blank pShuttle-CMV plasmid (vector) or pShuttle-H1-nonspecific scramble shRNA plasmid (sh-NC). After 6 h of transfection, the medium was replaced with fresh basal medium, and the culture was continued for 48 h. Transfection efficiency, cell viability, and iron concentration were then determined *via* Western blotting assays.

Cell viability assay

Cell viability was measured using a CCK-8 kit (Beyotime, Shanghai, China) according to the manufacturer's instructions. Briefly, cells were seeded in a 96-well plate at a density of 2.0×10^3/well. After each group of cells underwent the specific treatment, 10 μL of the CCK-8 reagent was added and incubated at 37 °C for 2 h. The absorbance of each sample was then evaluated using a microplate reader at 450 nm (Tecan, Switzerland).

Iron quantification

Initially, cells were seeded at a density of 5×10^6 cells per plate, and each group was processed as required. Then, an iron detection kit (ab83366, Abcam) was used following the manufacturer's protocol. The cells were rinsed with ice-chilled PBS and homogenized (on ice) using an iron assay buffer that was five times the volume of the cell solution. The resultant mixture was then centrifuged at 13,000×*g* and 4 °C for 10 min to remove any insoluble material. The supernatant was collected, and each sample was treated with an iron reducer, mixed, and left undisturbed at room temperature for 30 min. Each sample was treated with 100 μL of the iron probe and mixed thoroughly either by pipetting or using a horizontal shaker. The reaction was allowed to progress for 60 min at room temperature, with the plate kept in the dark. A microplate reader was used to determine the intracellular ion concentration at 593 nm.

Analysis of the production of reactive oxygen species (ROS)

After the cells were treated with $CoCl_2$ in the absence or presence of iohexol, the superoxide indicator dihydroethidium (5 μM; DHE, Invitrogen) was added to the culture medium. The cells were then incubated at 37 °C for 1 h. Nuclei were stained with DAPI. Fluorescence was observed under a fluorescence microscope (Revolve, Echo, San Diego, California, USA) and qualitatively analyzed. The excitation wavelength was 485 nm, and the emission wavelength was 527 nm.

Determination of ferroptosis by measuring lipid peroxides

To visualize lipid ROS, cells were treated with 2 μmol/L of the C11-BODIPY581/591 probe (Molecular Probes Inc.) and incubated in the dark at 37 °C for 30 min. Subsequently, DAPI (G1012; Servicebio) was used to stain the cell nuclei. Afterward, the cells were washed and analyzed using Liperfluo, and the fluorescence intensity of C11-BODIPY581/591 was determined.

RNA isolation and real-time PCR

RNA was extracted from each group of tissues using an RNA extraction kit (Qiagen). Reverse transcription and quantitative PCR were performed following the instructions provided with the TAKARA (Dalian, China) reverse transcription and RT-PCR kit. The primers were as follows: *Hp*, 5′-AAACTCCCCGAATGTGAGGC-3′ (F), 5′-TCCATAGAGCCACCGATGATG-3′ (R); *GAPDH*, 5′-AGCTTCGGCACATATTTCATCTG-3′ (F), and 5′-CGTTCACTCCCATGACAAACA-3′ (R). The data were normalized to *GAPDH* and calculated using the $2^{-\Delta\Delta Ct}$ method.

Western blotting analysis

Western blotting analysis was performed to detect the expression of the Hp and GAPDH proteins in kidney tissues and in HK-2 cells. The tissues or cells were routinely lysed to extract proteins. The BCA protein quantification kit (Thermo, USA) was used to quantify the extracted proteins. Conventional electrophoresis, membrane transfer, and antigen blocking were performed. Primary antibodies (dilutions: Hp (1:1000, EPR22856-212) and GAPDH (1:1000, ab8245)) were incubated with tissue sections overnight at 4 °C. The following day, the sections were washed and incubated with a secondary antibody. The Tianneng imaging agent (Tianneng, Shanghai, China) was used to visualize the protein bands. All experiments were repeated in triplicate.

Immunofluorescence staining

Immunofluorescence double staining was performed to stain specific proteins expressed in kidney tissues from each group of mice, including E-cadherin and Hp. After the routine processes and before incubating with antibodies, the sections were placed in a 10% BSA humidified box and sealed in an incubator at 37 °C for 30 min. The sections were then incubated overnight at 4 °C with diluted primary antibodies for E-cadherin (1:200, ab76055) and Hp (1:200). The next day, the slides were washed thrice with PBS (5 min per wash). Then, the cy3 or FITC-labeled fluorescent secondary antibodies (that matched the primary antibody) were added to the sections and incubated for 2 h. An anti-fluorescence quencher was added to the sections. Finally, the images were analyzed under a fluorescence microscope.

Statistical analysis

All experiments requiring statistical analysis were repeated in triplicate. Data are presented as the mean ± standard errors. Kruskal–Wallis one-way analysis of variance (ANOVA) was performed using SPSS software (version 13.0, SPSS, USA). All differences among and between groups were considered statistically significant at $p < 0.05$.

Results

$CoCl_2$ decreased renal function indicators after CIN

After administering cobalt chloride, we tested the levels of BUN, sCr, urinary urea, and urinary Cr in each group of mice. Following the addition of the contrast agent, the levels of BUN and sCr increased significantly, persisting until 72 h post-operation. The levels of BUN and sCr in the $CoCl_2$ group were significantly lower than those in the CIN group after 24 h of modeling and remained so for 72 h (Fig. 1B–E). The levels of urinary urea and urinary Cr were significantly lower in the CIN group but increased significantly after $CoCl_2$ treatment.

$CoCl_2$ attenuated the renal tubular damage caused by CIN

We performed H&E staining on kidney tissues from each group. The stained samples showed prominent damage to the renal tubules in the model group, which included erythrocyte stasis in the renal tubules or corpuscles (red arrow), shedding of epithelial cells (green arrow), changes in the basement membrane (black arrow), and flattening of renal tubular cells due to tubular dilation (orange arrows). Renal injury was considerably less pronounced in the $CoCl_2$ group (Fig. 2A). PAS staining yielded similar results. Tubule injury, characterized by cellular infiltration (red arrow) and dilated tubules with brush border loss (green arrows), epithelial flattening, and intratubular debris (black arrows), was evident in the contrast-induced model. However, $CoCl_2$ treatment ameliorated this injury. Consistent changes in the injury score among groups also indicated the renoprotective effects of $CoCl_2$ (Fig. 2B). We co-stained renal tubular cells with E-cadherin and TUNEL to assess cell death and observed that the number of TUNEL-positive renal tubular cells increased significantly in the model group. Yet, after $CoCl_2$ treatment, the number of positive cells decreased significantly (Fig. 3).

Quantitative proteomic analysis of kidney tissues from CIN mice receiving $CoCl_2$ treatment

To elucidate the mechanism underlying the action of $CoCl_2$ on CIN, protein extracts from the kidneys of mice treated with or without $CoCl_2$ were analyzed by TMT. After merging duplicated data, 5455 proteins were identified, with 79 being differentially expressed proteins (DEPs) between the model and $CoCl_2$ groups (Fig. 4A and Supplementary Table S1). Through GO and KEGG pathway enrichment analyses, we discerned that these 79 proteins were primarily enriched in the homeostasis of several cell types (biological process, BP), the basal part of the cell (cell component, CC), and hemoglobin (Hb) binding (molecular function); including protein digestion and absorption, the ECM-receptor pathway, the PPAR signaling pathway, and steroid biosynthesis. Upon reviewing the literature, we noticed that some terms were associated with ferroptosis, which are enclosed in dotted lines (Fig. 4B and C). We then identified proteins that also changed differentially after iohexol induction, identifying 28 such proteins (Fig. 4D). Except for A2NW55, the remaining 27 proteins were all annotated: Krt78, Iigp1, Krt1, Col4a5, Hbb-b2, Col6a1, Acmsd, Slc43a1, Hbbt1, Arhgap12, Slc4a1, Cyp2e1, Bpgm, Alas1, Sptb, Cyp2d22, Adgrg1, Prss1, Pla2 g7, Flot2, Stfa2, Cd74, Nsmce1, Hmgcs2, Cyp4a14, Hp, and Gda. These proteins underwent GO and KEGG pathway enrichment analyses. The results revealed some terms associated with ferroptosis (enclosed in dashed boxes; Fig. 4E and F). After conducting the GO and KEGG pathway analyses for the 27 overlapping proteins, the terms related to ferroptosis were highlighted in a heatmap (Fig. 4G). We observed that five proteins (Cyp2d22, Pla2 g7, Sqle, Hp, and Cyp4a14) increased post-contrast induction and decreased after $CoCl_2$ treatment, whereas the others did not follow this pattern. Therefore, we further analyzed them, noting that Sqle is a regulator of ferroptosis[17] and Hp is also associated with it,[18–20] but no published study has shown the relationship between other proteins and ferroptosis. Considering that Sqle plays a role in ferroptosis,[17] and as Hp has a relatively uncertain function in ferroptosis, we selected Hp for further investigation, although our results showed that Hp did not have a high degree of connectivity in the PPI network of the 79 DEPs or the 27 overlapping DEPs (Supplementary Fig. S1).

The expression levels of Hp decreased in CIN mice after treatment with $CoCl_2$

To validate the results of the proteomics analysis, we conducted Western blotting and qPCR analyses to assess the expression of Hp's protein and mRNA in kidney tissues from the experimental mice. Our findings indicated that the protein level of Hp was notably higher in the model group than in the normal group. However, after $CoCl_2$ administration, Hp's protein levels decreased (Fig. 5A). The mRNA level changes mirrored those observed in the protein levels (Fig. 5B). Dual fluorescent labeling was used to determine the expression level of Hp in renal tubular cells, aligning with the results from the TMT data (Fig. 5C). Based on these outcomes (Fig. 4), we deduced that Hp was intricately linked with ferroptosis. We then investigated cell viability, iron concentration, and ROS content in renal tissues to confirm whether CIN and $CoCl_2$ are associated with ferroptosis. Our research established that cell viability decreased while iron concentration and ROS content increased in the renal tissues of CIN-afflicted mice. However, $CoCl_2$ treatment partially reversed these effects, implying a potential relationship between CIN, $CoCl_2$ treatment, and ferroptosis.

$CoCl_2$ plays a protective role in CIN by inhibiting ferroptosis by upregulating Hp in vitro

HK-2 cells were utilized, along with Hp-interference and overexpression adenoviruses, to investigate the correlation

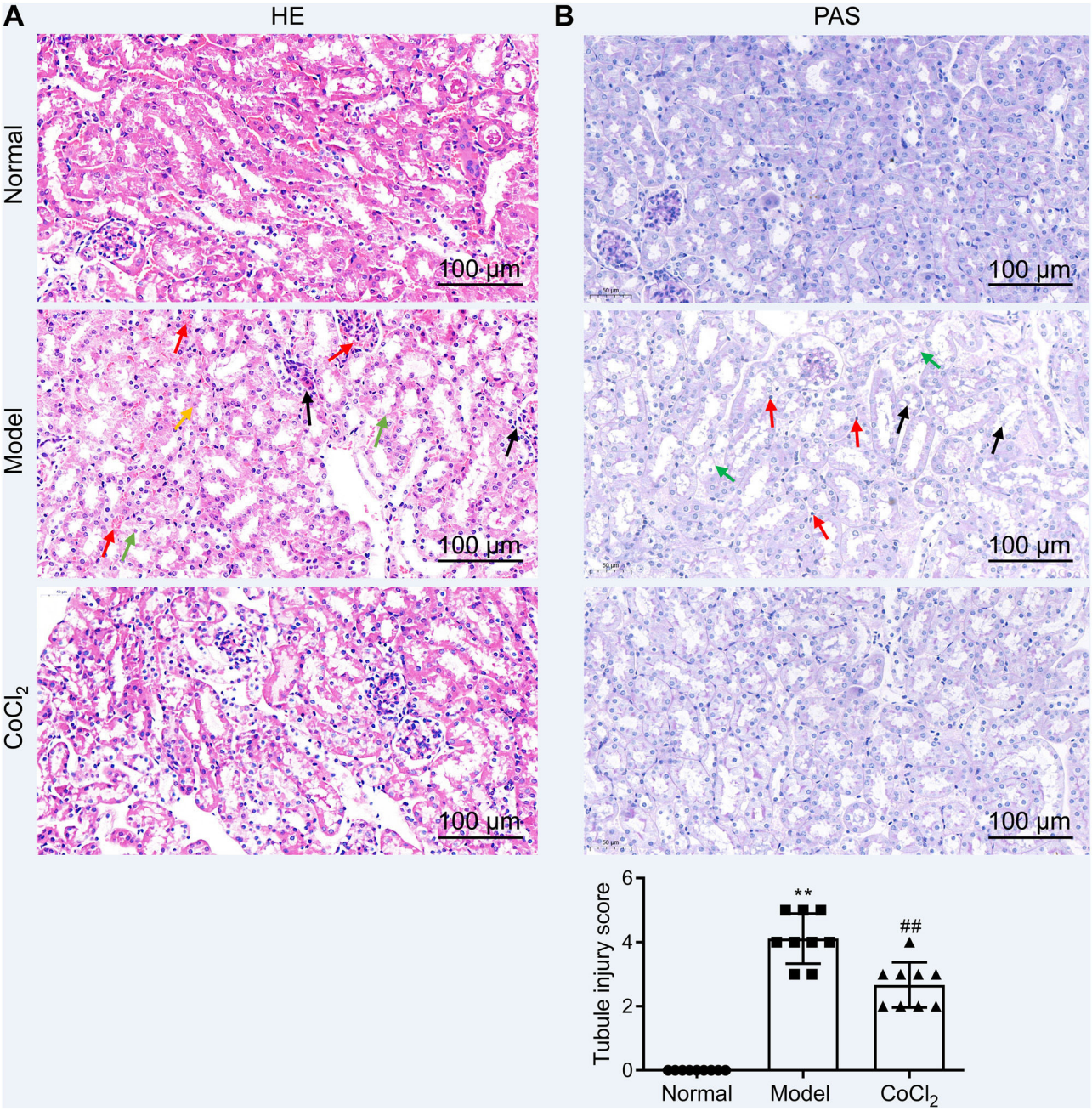

Fig. 2 – Histopathological analysis after treatment. (A) H&E staining depicting kidney features. Model group exhibited erythrocyte stasis (red arrow), epithelial cell shedding (green arrow), bare basement membrane (black arrow), and renal tubular cell flattening due to dilation (orange arrows). $CoCl_2$ group showed lesser damage than CIN group. (B) Periodic acid-Schiff staining: magnification, 400×. * indicateds model vs. normal, # indicates $CoCl_2$ vs. model; n = 9; **,## p < 0.01.

between Hp and ferroptosis, as well as the potential role of Hp in the anti-CIN treatment with $CoCl_2$. The efficiency of knockdown and/or overexpression strategies was assessed at both the transcriptional and translational levels following adenovirus infection (Fig. 6A and Fig. S2A–B). *In vivo* findings indicated a possible positive association between Hp and ferroptosis. However, when Hp was overexpressed *in vitro*, cell viability increased, a change that remained largely unaffected by the ferroptosis inhibitor ferrostatin-1 (Fer-1), which targets the 15LOX-PEBP1 complex and lipid peroxidation (Fig. S2C). To corroborate our observations, we assessed Fe concentration, ROS levels, and the expression of ferroptosis markers GPX4 (glutathione peroxidase 4) and SLC7A11 (solute carrier family 7 member 11). The results demonstrated that Hp inhibited ferroptosis without inducing iron overload, and this inhibition remained unaffected by Fer-1 (Fig. S2D–F). Consequently, Hp was deemed a ferroptosis suppressor. Subsequent experiments involved the use of erastin to induce ferroptosis in HK-2 cells. Erastin treatment reduced cell viability, an effect counteracted by *Hp* overexpression but exacerbated by *Hp*

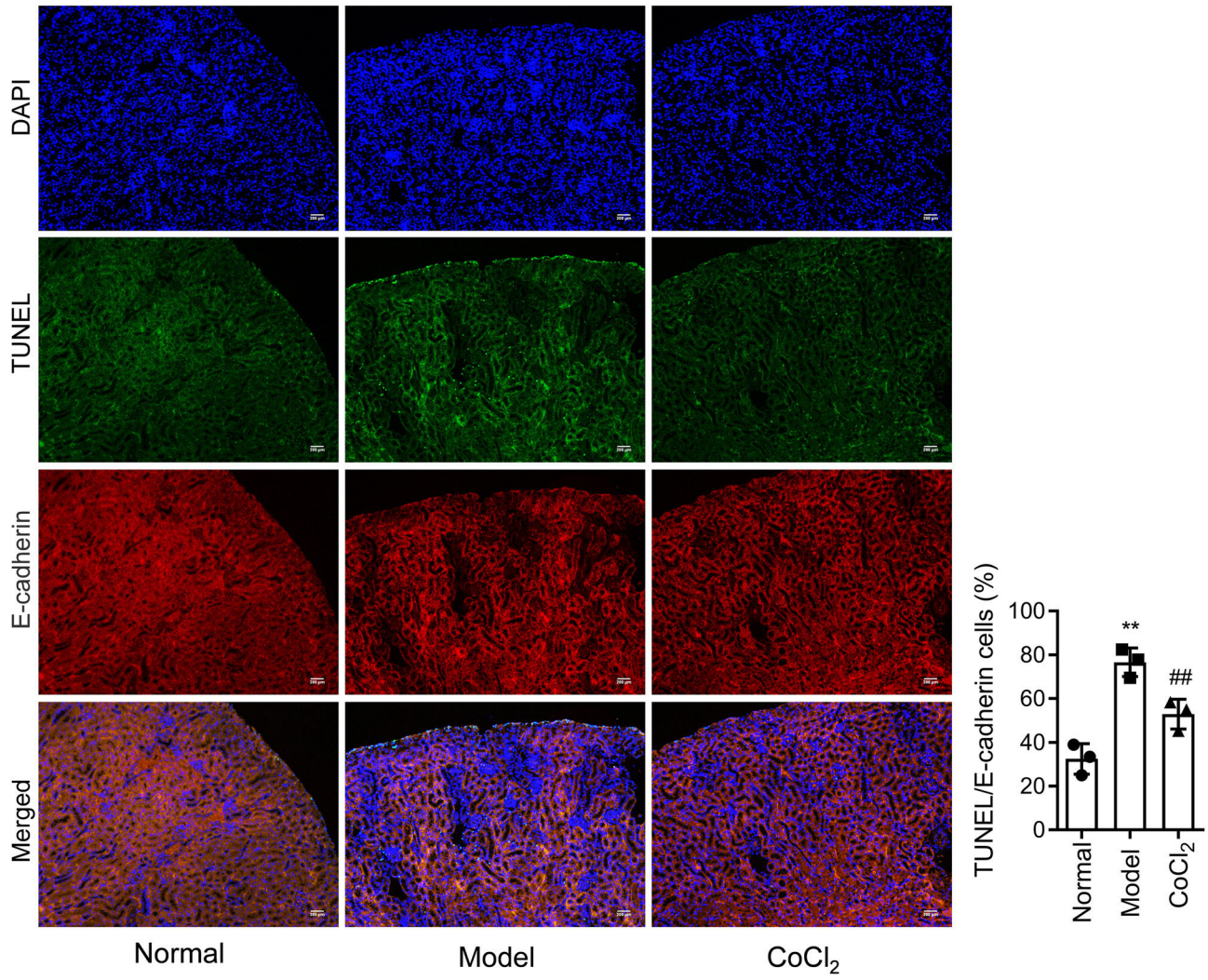

Fig. 3 – Co-staining using E-cadherin and TUNEL to detect apoptosis in renal tubular cells. Fluorescence intensity analyzed to assess renal tubule cell apoptosis; * indicates model *vs.* normal; # indicates $CoCl_2$ *vs.* model; $n = 6$; **,## $p < 0.01$.

knockdown (Fig. 6B). Post-erastin treatment, cellular iron and ROS levels in HK-2 cells significantly increased. Notably, *Hp* overexpression markedly reduced iron and ROS levels, while *Hp* knockdown resulted in their significant elevation (Fig. 6C and D). *Hp* knockdown increased erastin-induced lipid oxidation, as indicated by increased green fluorescence intensity (reflecting levels of oxidized C11 BODIPY 581/591), while *Hp* overexpression diminished fluorescence intensity (Fig. 6E). Furthermore, protein levels of two typical ferroptosis biomarkers, Gpx4 and Slc7a11, decreased upon *Hp* knockdown and increased upon *Hp* overexpression following erastin treatment (Fig. 6F).

For creating an *in vitro* cellular model of CIN, HK-2 cells were treated with iohexol. $CoCl_2$, in conjunction with Hp-interference or overexpression adenoviruses, was then employed to investigate whether $CoCl_2$ can counteract CIN by modulating ferroptosis *via* Hp. The cellular activity of the CIN model group significantly decreased, while iron concentration and ROS content markedly increased. Following administration of $CoCl_2$ or *Hp* overexpression, cell viability substantially increased, while iron concentration and ROS content significantly decreased compared to the CIN group (Fig. 6G–I). Lipid oxidation levels increased in the CIN group; however, after $CoCl_2$ treatment or *Hp* overexpression, fluorescence intensity notably decreased (Fig. 6J). Changes in Gpx4 and Slc7a11 protein levels exhibited inverse patterns (Fig. 6K), thus, supporting the aforementioned findings (Fig. 6G–J). Conversely, *Hp* knockdown exhibited opposing effects on the above-mentioned ferroptosis indicators in the CIN *in vitro* model treated with $CoCl_2$ (Fig. 6G–K).

Discussion

In this study, we employed a mouse model of CIN to demonstrate that $CoCl_2$ significantly mitigates kidney damage, renal tubular damage, and epithelial cell death associated with CIN. Subsequently, we conducted quantitative proteomics and bioinformatics analyses to identify and examine key proteins linked to contrast-induced renal damage. Western blotting assays validated changes in candidate protein expression identified through proteomics. Utilizing erastin to induce

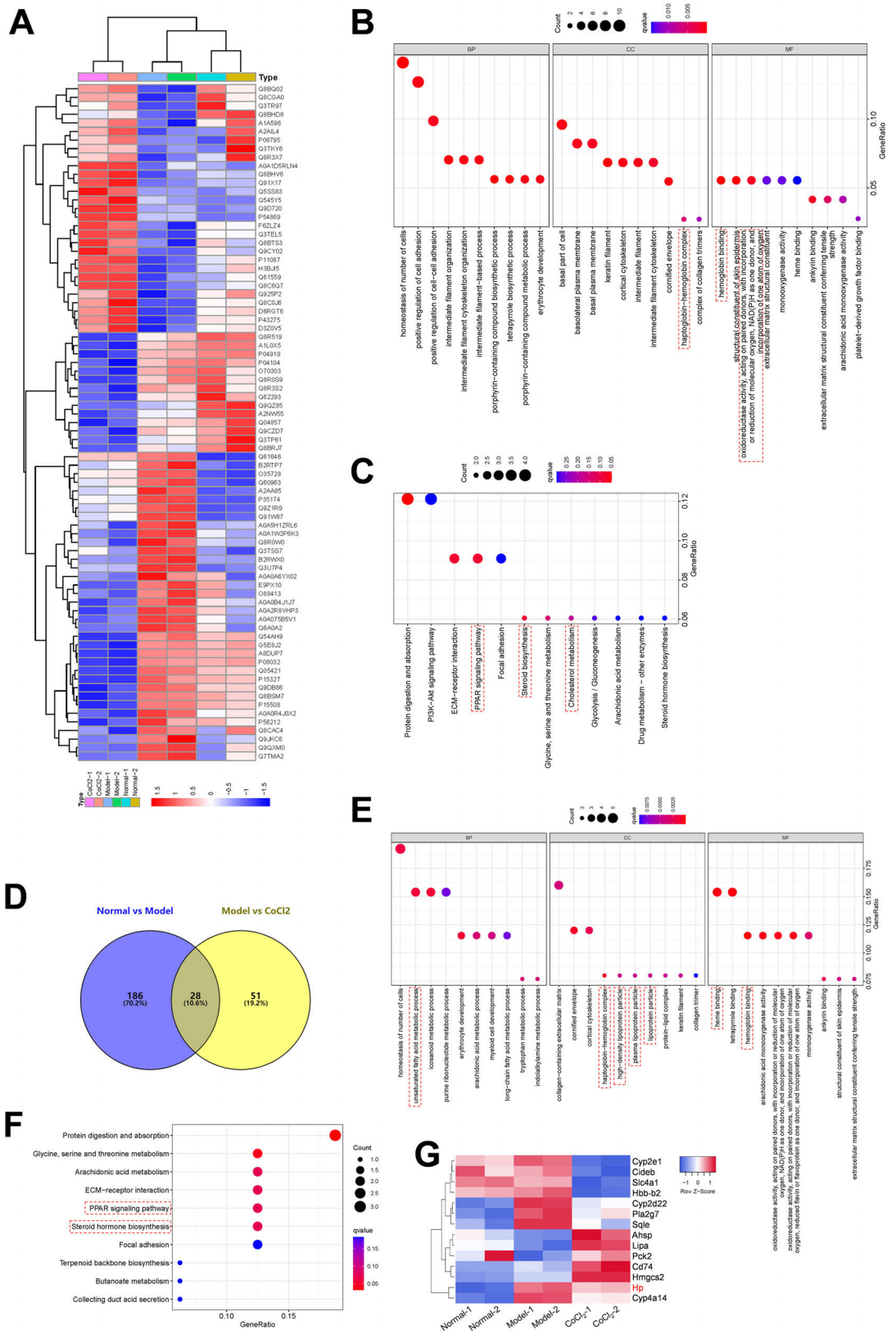

Fig. 4 – Differentially expressed proteins (DEPs) and their GO and KEGG pathway analyses. (A) Heatmap of 79 DEPs (model *vs.* $CoCl_2$ treatment) across all groups. (B and C) GO (B) and KEGG pathway (C) analyses of 79 DEPs. (D) Venn diagram of proteins overlapping between normal *vs.* model and model *vs.* $CoCl_2$ comparisons. (E and F) GO (E) and KEGG pathway (F) analyses of 79 overlapped DEPs. (G) Proteins enriched in GO or KEGG pathways related to ferroptosis were selected; their expression among three groups is shown in the heatmap. Terms outlined with dotted lines were associated with ferroptosis based on published data.

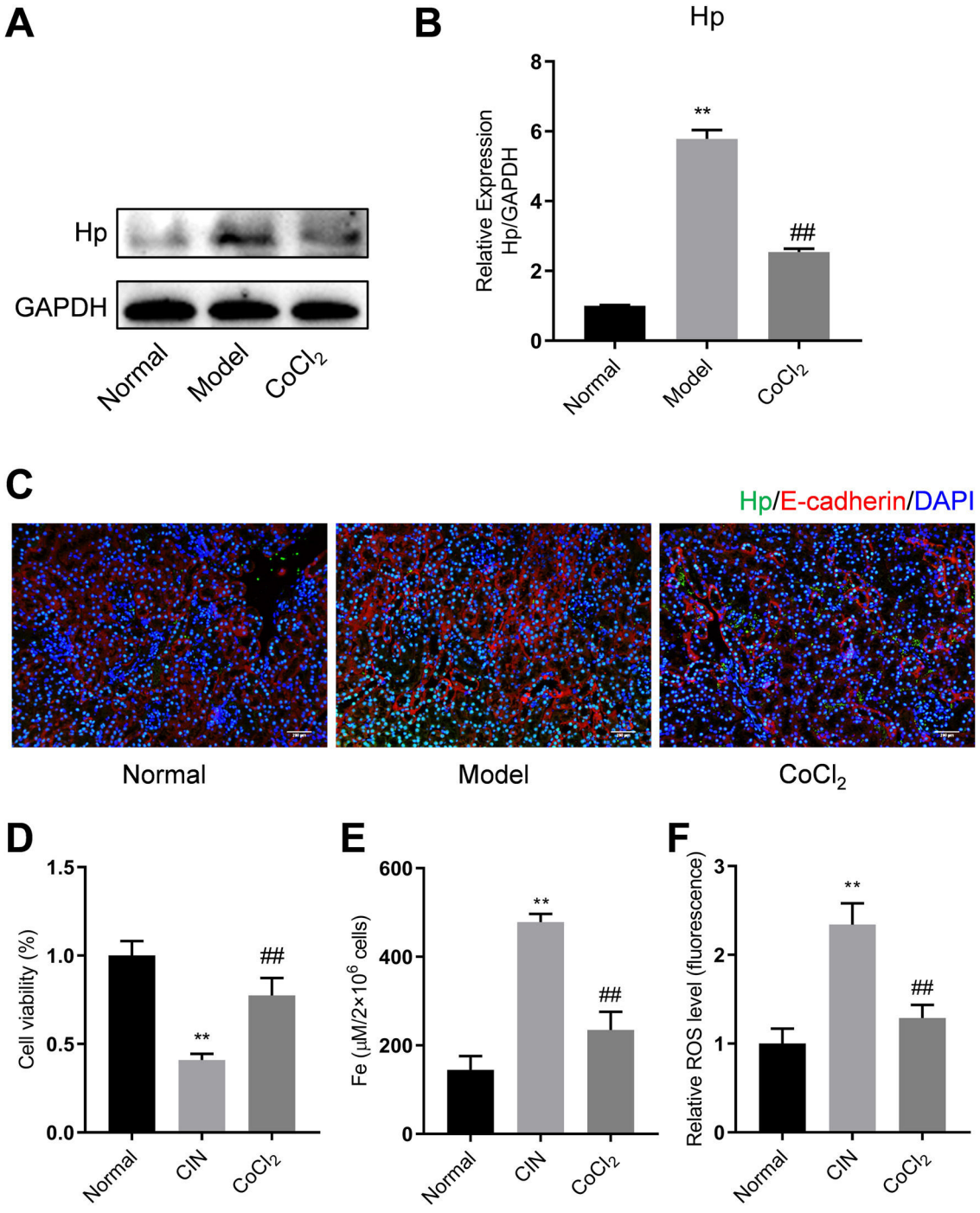

Fig. 5 – Western blotting, qPCR, and IF analyses of Hp from mouse kidney tissues. (A) Proteins tested thrice and normalized to GAPDH levels for quantitative analysis. (B) Quantitative analysis of Hp mRNA expression. IF co-stained four proteins and E-cadherin in renal tubular epithelial cells (C, magnification, 200×). (D–F) Cell viability, iron concentration, and ROS content estimated for ferroptosis levels. Each value represents mean ± SD; * indicates model *vs.* normal; # indicates $CoCl_2$ *vs.* model; $n = 6$; *,# $p < 0.05$; **,## $p < 0.01$.

ferroptosis, we elucidated the interplay between Hp and ferroptosis. Lastly, we employed the HK-2 CIN cell model and adenovirus-overexpressing Hp to confirm that $CoCl_2$ safeguards renal epithelial cells from contrast-induced injury by attenuating ferroptosis, in which Hp likely participates by influencing intracellular ferrous concentration. These findings offer theoretical backing for $CoCl_2$'s protective effect on renal tubules after CIN.

The pathogenesis of CIN is intricate and encompasses hemodynamic shifts, ischemia, oxidative stress, and inflammation. Administration of CM prompts the synthesis of vasoconstrictors (*e.g.*, endothelin, adenosine, thromboxane

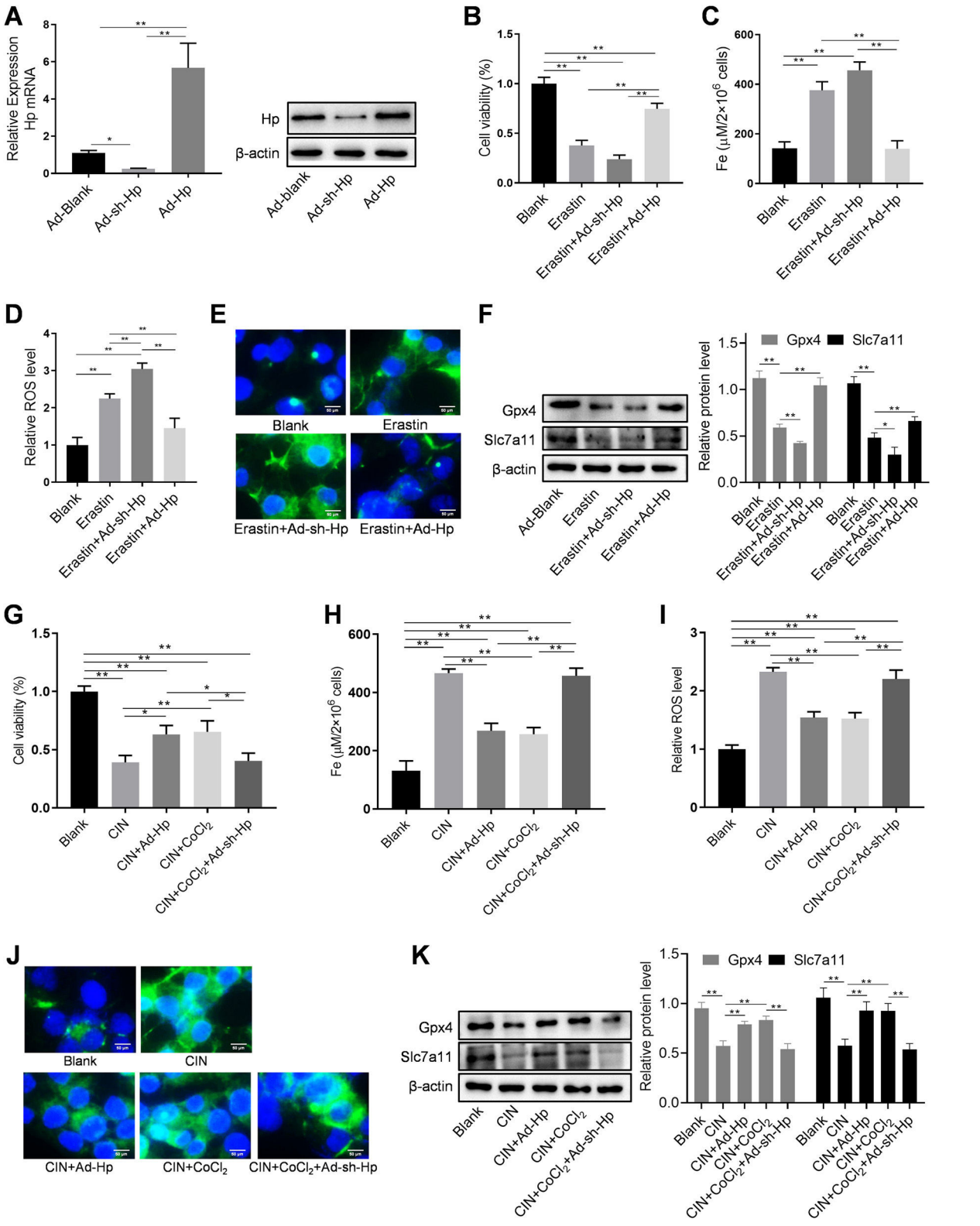

Fig. 6 – $CoCl_2$'s protective effect against CIN by regulating ferroptosis *via* Hp targeting. (A) Western blotting and qPCR to detect adenovirus transfection efficiency. Erastin-induced ferroptosis and Hp-interference/overexpression adenoviruses were transfected. (B–D) Cell viability, iron concentration, and ROS content estimated for ferroptosis level. (E) Ferroptosis analysis using C11-BODIPY581/591 fluorescence. (F) Western blotting of ferroptosis biomarkers GPX4 and SLC7A11 after erastin treatment with *Hp* overexpression or silencing. (G–I) Iohexol treated HK-2 cells to create CIN cellular model; $CoCl_2$ or Hp-interference/overexpression adenoviruses applied. Cell viability, iron concentration, and ROS content measured for ferroptosis levels. (J) Ferroptosis analysis using C11-BODIPY581/591 fluorescence. (K) Western blotting of ferroptosis biomarkers Gpx4 and Slc7a11. Each value represents mean ± SD; $^{*}p < 0.05$ and $^{**}p < 0.01$.

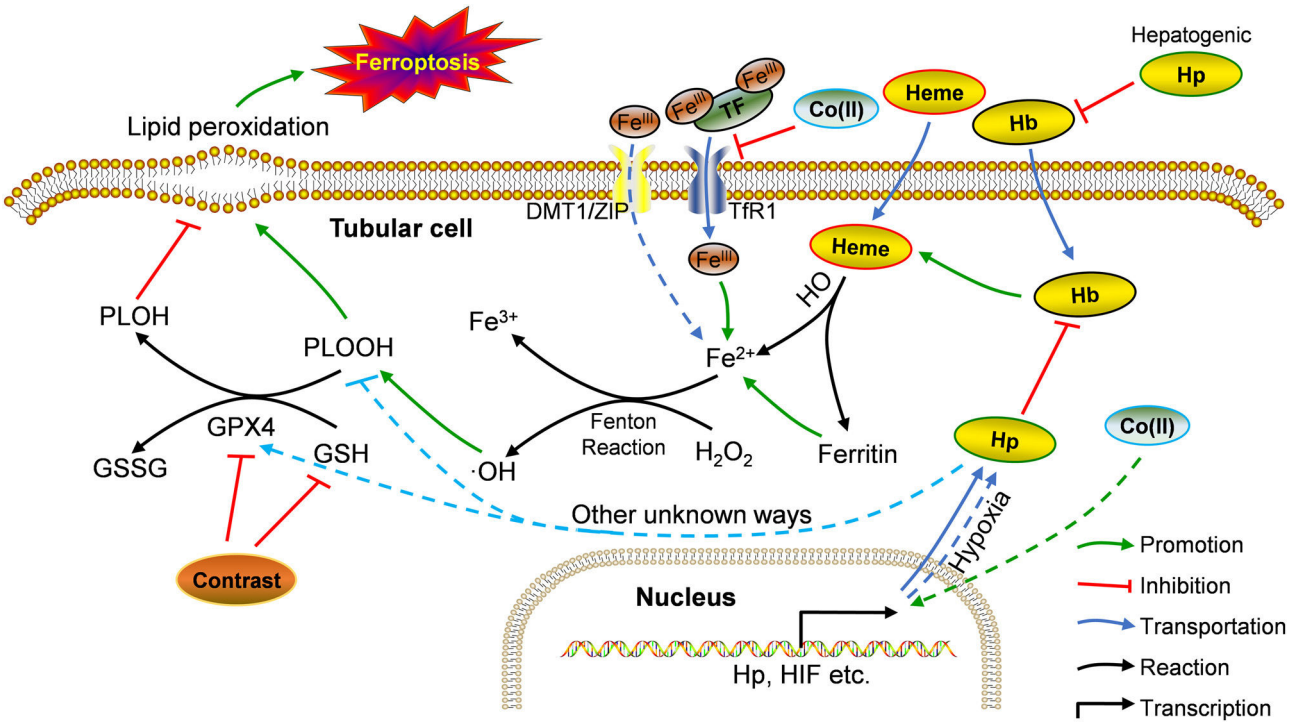

Fig. 7 – Potential mechanism of Hp's involvement in CIN treatment using $CoCl_2$. Co: cobalt; DMT1: divalent metal transporter 1; GPX4: glutathione peroxidase 4; GSSG: glutathione disulfide; Hb: hemoglobin; Hp: haptoglobin; HO: heme oxygenase; PLOH: phospholipid alcohols; PLOOH: phospholipid hydroperoxides; TF: transferrin; TfR1: transferrin receptor 1; ZIP: zinc-regulated transporter/iron-regulated transporter-like protein. Solid line: *in vivo*; dotted line: *in vitro*.

A2) and a reduction in vasodilators (*e.g.*, nitric oxide), leading to renal blood vessel contraction, potentially resulting in ischemic necrosis of renal tubular cells.[21] High-viscosity plasma induced by hypotonic contrast agents can lead to renal tubule damage through hypoperfusion and tubule blockage.[22] Contrast agents directly inflict toxic damage on renal tubular cells, causing calcium ion accumulation, ROS-mediated DNA fragmentation, mitochondrial dysfunction, and various forms of cell death.[8,23] Mitochondrial damage stimulates ROS production, causing oxidative DNA damage and escalating the production of inflammasomes containing protein three pyrimidine domain (NLRP3).[24] Contrast agents also induce renal hypoxia, redox reaction imbalances, and increased ROS levels.[25,26] Recent studies have highlighted CM's capacity to induce ferroptosis in renal tubular epithelial cells and kidney tissues, characterized by lipid metabolite homeostasis disruption and reduced GSH and GPX4 levels.[27,28] Given these findings and the perturbations in redox reactions, ROS, and oxidase, we focused on ferroptosis, which is deemed crucial in CIN.[29]

Renal ischemia and hypoxia ensuing from CM administration underlie CIN. Hypoxic preconditioning enhances cellular tolerance to hypoxic stress, mitigating the adverse effects of hypoxia on cells.[11] $CoCl_2$, a HIF-1α activator, safeguards against renal tubular damage.[12] A study demonstrated that $CoCl_2$ treatment of HK-2 cells curtailed inflammation and ROS production.[13] ROS significantly impact CIN, with their accumulation pivotal for cellular ferroptosis. This prompts a pertinent query: does $CoCl_2$'s hypoxic effect shield renal tubular cells and impact ferroptosis? We addressed this issue by conducting a TMT proteomic analysis of kidney tissue from CIN-afflicted mice treated with $CoCl_2$. Subsequently, traditional molecular experiments identified Hp as a potential key DEP. Western blotting and qPCR findings correlated with TMT-based proteomics outcomes. While Hp was prominently expressed in the CIN model, $CoCl_2$ treatment attenuated its expression.

Our *in vivo* and *in vitro* findings seemingly juxtaposed each other. Drawing from previous research and our observations, we propose the following rationale (summarized in Fig. 7): *in vivo*, under physiological conditions, hemoglobin and heme release Fe^{2+} into cells, fostering the Fenton reaction and elevating •OH and PLOOH (phospholipid hydroperoxides) levels.[30] GPX4 and GSH counterbalance this process, reducing PLOOH to PLOH (phospholipid alcohols), thereby sustaining equilibrium.[31] Contrast agents diminish GPX4 and GSH levels, instigating ferroptosis in renal tubular cells.[32] During ferroptosis, Hp strongly binds to free Hb, curbing its oxidative activity, its role in ferroptosis, and the resulting renal injury.[33,34] Hb could also suppress iron accumulation in tubular cells, thus, ameliorating Fenton reaction-related iron storage abnormalities, ROS production, and/or ultimate ferroptosis.[35,36] After $CoCl_2$ treatment, reduced iron-transferrin binding results in decreased intracellular iron levels,[37] consequently mitigating intracellular Fe^{2+}-induced ferroptosis. This likely causes a decline in required Hp, potentially due to a direct reduction in hepatocyte-derived Hp (given the liver's primary Hp source,[38] forming a systemic feedback regulation mechanism). Sup-

porting this speculation, reports indicate decreased plasma haptoglobin levels post-$CoCl_2$ treatment.[32] Conversely, Co (II) can mimic hypoxia-like phenotypes by stabilizing HIF-1α,[37] possibly leading to enhanced Hp transcription and expression in cobalt-induced tubular cells.[39] *In vitro*, tubular cells directly acquire intracellular iron from the culture medium (typically containing Fe^{3+} and Fe^{2+}), sans Hb, resulting in a disparity from the *in vivo* environment. This highlights unknown pathways governing Hp-mediated ferroptosis regulation in tubules post-$CoCl_2$ treatment. Notably, altered levels of other ferroptosis-related proteins were observed (Fig. 4), warranting further investigation.

Due to ferroptosis's complexity and resource limitations, our study had some shortcomings. First, other crucial molecules (Cyp2d22, Pla2 g7, Sqle, Cyp4a14), important in ferroptosis, were not explored. Second, the small animal sample size may have introduced data heterogeneity and invalidated conclusions. Additionally, we omitted the group of mice solely treated with $CoCl_2$ in the absence of iohexol. This omission could complicate the understanding of reciprocal iohexol and $CoCl_2$ effects, necessitating a cautious interpretation.

Considering multiple molecular studies on $CoCl_2$'s CIN treatment potential, and despite these limitations, $CoCl_2$ might have promising clinical prospects. However, an essential consideration emerges: $CoCl_2$'s carcinogenicity arises from its capacity to elevate hypoxia-inducible factor-1α (HIF-1α) expression, a pivotal regulator of tumor survival, metastasis, and angiogenesis.[40,41] Furthermore, $CoCl_2$ and exogenous genotoxin co-exposure could enhance genetic instability.[42] Consequently, the clinical use of $CoCl_2$ for CIN treatment requires refinement.

Conclusion

In summary, our study revealed that $CoCl_2$ reduced markers of kidney damage post-CIN and alleviated renal tubular injury induced by CIN. Quantitative proteomic analysis of kidney tissue from CIN-infected mice treated with $CoCl_2$ unveiled its potential to exert therapeutic benefits *via* diverse proteins, targets, and pathways within the CIN mouse model. $CoCl_2$'s protective role against CIN-induced renal tubular cell death was validated, and these outcomes were linked to Hp-mediated suppression of ferroptosis.

Funding

This research was supported by National Natural Science Foundation of China (Grant Number: 82170713), Natural Science Foundation of Shanghai (Grant Number: 19ZR1433300), Shanghai Municipal Health Commission Research Project (Grant Number: 202040293), and the Project of Medical Guidance (Chinese and Western Medicine) of Science and Technology Commission of Shanghai Municipality (Grant Number: 134119a5700).

Conflicts of interest

None declared.

Acknowledgement

The language of this study was professionally edited by ExEditing.com.

Appendix A. Supplementary data

Supplementary data associated with this article can be found, in the online version, at doi:10.1016/j.nefro.2023.08.007.

REFERENCES

1. Nash K, Hafeez A, Hou S. Hospital-acquired renal insufficiency. Am J Kidney Dis. 2002;39:930–6.
2. Weisbord SD, Gallagher M, Jneid H, Garcia S, Cass A, Thwin S-S, et al. Outcomes after angiography with sodium bicarbonate and acetylcysteine. N Engl J Med. 2018;378:603–14.
3. van der Molen AJ, Reimer P, Dekkers IA, Bongartz G, Bellin M-F, Bertolotto M, et al. Post-contrast acute kidney injury – part 1: definition, clinical features, incidence, role of contrast medium and risk factors. Eur Radiol. 2018;28:2845–55.
4. Hossain MA, Costanzo E, Cosentino J, Patel C, Qaisar H, Singh V, et al. Contrast-induced nephropathy: pathophysiology, risk factors, and prevention. Saudi J Kidney Dis Transpl. 2018;29:1.
5. Faucon A-L, Bobrie G, Clément O. Nephrotoxicity of iodinated contrast media: from pathophysiology to prevention strategies. Eur J Radiol. 2019;116:231–41.
6. Sonali G, Pradeep G, Nishant G, Harpreet S, Vivek K. Contrast-induced nephropathy: current practice. J Urol Nephrol Stud. 2018;1:9–19.
7. Shen J, Wang L, Jiang N, Mou S, Zhang M, Gu L, et al. NLRP3 inflammasome mediates contrast media-induced acute kidney injury by regulating cell apoptosis. Sci Rep. 2016;6:1–10.
8. Samadian F, Dalili N, Mahmoudieh L, Ziaei S. Contrast-induced nephropathy: essentials and concerns. Iran J Kidney Dis. 2018;12:135.
9. Solomon R, Gordon P, Manoukian SV, Abbott JD, Kereiakes DJ, Jeremias A, et al. Randomized trial of bicarbonate or saline study for the prevention of contrast-induced nephropathy in patients with CKD. Clin J Am Soc Nephrol. 2015;10:1519–24.
10. Iranirad L, Hejazi SF, Sadeghi MS, Jang SA. Efficacy of nicorandil treatment for prevention of contrast-induced nephropathy in high-risk patients undergoing cardiac catheterization: a prospective randomized controlled trial. Cardiol J. 2017;24:502–7.
11. Eckardt K-U, Rosenberger C, Jürgensen JS, Wiesener MS. Role of hypoxia in the pathogenesis of renal disease. Blood Purif. 2003;21:253–7.
12. Tanaka T, Kojima I, Ohse T, Ingelfinger JR, Adler S, Fujita T, et al. Cobalt promotes angiogenesis via hypoxia-inducible factor and protects tubulointerstitium in the remnant kidney model. Laboratory Investigation. 2005;85:1292–307, http://dx.doi.org/10.1038/labinvest.3700328.
13. Oh SW, Lee YM, Kim S, Chin HJ, Chae DW, Na KY. Cobalt chloride attenuates oxidative stress and inflammation through NF-κB inhibition in human renal proximal tubular epithelial cells. J Korean Med Sci. 2014;29 Suppl. 2:S139–45, http://dx.doi.org/10.3346/jkms.2014.29.S2.S139.
14. Altintop I, Tatli M, Karakukcu C, Soyer Sarica Z, Hanım Yay A, Balcioglu E, et al. Serum and tissue HIF-2 alpha expression in CIN, N-acetyl cysteine, and sildenafil-treated rat models: an

experimental study. Medicina (Kaunas, Lithuania). 2018;54, http://dx.doi.org/10.3390/medicina54040054.
15. Oh G-S, Kim H-J, Choi J-H, Shen A, Choe S-K, Karna A, et al. Pharmacological activation of NQO1 increases NAD+ levels and attenuates cisplatin-mediated acute kidney injury in mice. Kidney Int. 2014;85:547–60, http://dx.doi.org/10.1038/ki.2013.330.
16. Orsburn BC. Proteome discoverer – a community enhanced data processing suite for protein informatics. Proteomes. 2021;9, http://dx.doi.org/10.3390/proteomes9010015.
17. Tang W, Xu F, Zhao M, Zhang S. Ferroptosis regulators, especially SQLE, play an important role in prognosis, progression and immune environment of breast cancer. BMC Cancer. 2021;21:1–19.
18. Wei Q, Zhang Y-T, Lin L-S, He E-J, He Y-Y, Su Y-H, et al. Haptoglobin suppresses hepatocyte ferroptosis via inhibition of the ERK1/2 signaling pathway. J Shanghai Jiaotong Univ (Med Sci). 2021;41:999.
19. Li G, Yang J, Zhao G, Shen Z, Yang K, Tian L, et al. Dysregulation of ferroptosis may involve in the development of non-small-cell lung cancer in Xuanwei area. J Cell Mol Med. 2021;25:2872–84.
20. Yang L, Cao L-M, Zhang X-J, Chu B. Targeting ferroptosis as a vulnerability in pulmonary diseases. Cell Death Dis. 2022;13:649, http://dx.doi.org/10.1038/s41419-022-05070-7.
21. Lamby P, Jung F, Falter J, Mrowietz C, Graf S, Schellenberg L, et al. Effect of radiographic contrast media on renal perfusion – first results. Clin Hemorheol Microcirc. 2016;64: 287–95.
22. Azzalini L, Spagnoli V, Ly HQ. Contrast-induced nephropathy: from pathophysiology to preventive strategies. Can J Cardiol. 2016;32:247–55.
23. Hosohata K, Harnsirikarn T, Chokesuwattanaskul S. Ferroptosis: a potential therapeutic target in acute kidney injury. Int J Mol Sci. 2022;23:6583.
24. Lin Q, Li S, Jiang N, Shao X, Zhang M, Jin H, et al. PINK1-parkin pathway of mitophagy protects against contrast-induced acute kidney injury via decreasing mitochondrial ROS and NLRP3 inflammasome activation. Redox Biol. 2019;26:101254.
25. Pisani A, Riccio E, Andreucci M, Faga T, Ashour M, Di Nuzzi A, et al. Role of reactive oxygen species in pathogenesis of radiocontrast-induced nephropathy. Biomed Res Int. 2013;2013:868321.
26. Su L, Zhang J, Gomez H, Kellum JA, Peng Z. Mitochondria ROS and mitophagy in acute kidney injury. Autophagy. 2022;19:1–14.
27. Fangfang Z, Lianxin L, Yixin C, Yi L, Qun L. Untargeted lipidomics reveals the potential mechanism of ferroptosis in HK-2 Cells treated with iohexol. AKI: mechanisms of injury. 2021 [Category: Acute Kidney Injury; Abstract: PO0385], https://www.asn-online.org/education/kidneyweek/2021/program-abstract.aspx?controlId=3606510
28. Fang D, Wang Y, Zhang Z, Yang D, Gu D, He B, et al. Calorie restriction protects against contrast-induced nephropathy via SIRT1/GPX4 activation. Oxid Med Cell Longev. 2021;2021:2999296, http://dx.doi.org/10.1155/2021/2999296.
29. Zhao Z, Wu J, Xu H, Zhou C, Han B, Zhu H, et al. XJB-5-131 inhibited ferroptosis in tubular epithelial cells after ischemia–reperfusion injury. Cell Death Dis. 2020;11:1–15.
30. Chiabrando D, Vinchi F, Fiorito V, Tolosano E. Haptoglobin and hemopexin in heme detoxification and iron recycling. In: Acute phase proteins – regulation and functions of acute phase protein; 2011. p. 261–88, https://doi.org/10.5772/18241
31. Bayır H, Dixon SJ, Tyurina YY, Kellum JA, Kagan VE. Ferroptotic mechanisms and therapeutic targeting of iron metabolism and lipid peroxidation in the kidney. Nat Rev Nephrol. 2023:1–22.
32. Ahmad Y, Mishra S, Arya A, Paul S, Sharma M, Prasad J, et al. Revisiting cobalt chloride preconditioning to prevent hypobaric hypoxia-induced damage: identification of global proteomic alteration and key networks. Funct Integr Genomics. 2016;16:281–95.
33. Tang D, Chen X, Kang R, Kroemer G. Ferroptosis: molecular mechanisms and health implications. Cell Res. 2021;31:107–25, http://dx.doi.org/10.1038/s41422-020-00441-1.
34. MacKellar M, Vigerust DJ. Role of haptoglobin in health and disease: a focus on diabetes. Clin Diabetes. 2016;34:148–57, http://dx.doi.org/10.2337/diaclin.34.3.148.
35. Fagoonee S, Gburek J, Hirsch E, Marro S, Moestrup SK, Laurberg JM, et al. Plasma protein haptoglobin modulates renal iron loading. Am J Pathol. 2005;166:973–83, http://dx.doi.org/10.1016/s0002-9440(10)62319-x.
36. Liu J, Kang R, Tang D. Signaling pathways and defense mechanisms of ferroptosis. FEBS J. 2022;289:7038–50.
37. Paustenbach DJ, Tvermoes BE, Unice KM, Finley BL, Kerger BD. A review of the health hazards posed by cobalt. Crit Rev Toxicol. 2013;43:316–62.
38. Bhensdadia NM, Hunt KJ, Lopes-Virella MF, Michael Tucker J, Mataria MR, Alge JL, et al. Urine haptoglobin levels predict early renal functional decline in patients with type 2 diabetes. Kidney Int. 2013;83:1136–43, http://dx.doi.org/10.1038/ki.2013.57.
39. Oh MK, Park HJ, Kim NH, Park SJ, Park IY, Kim IS, et al. Hypoxia-inducible factor-1alpha enhances haptoglobin gene expression by improving binding of STAT3 to the promoter. J Biol Chem. 2011;286:8857–65, http://dx.doi.org/10.1074/jbc.M110.150557.
40. Mavrofrydi O, Papazafiri P. Hypoxia-inducible factor-lα increase is an early and sensitive marker of lung cells responding to benzo[a]pyrene. J Environ Pathol Toxicol Oncol. 2012;31:335–47, http://dx.doi.org/10.1615/jenvironpatholtoxicoloncol.v31.i4.40.
41. Zhong H, Hanrahan C, van der Poel H, Simons JW. Hypoxia-inducible factor 1alpha and 1beta proteins share common signaling pathways in human prostate cancer cells. Biochem Biophys Res Commun. 2001;284:352–6, http://dx.doi.org/10.1006/bbrc.2001.4981.
42. Schults MA, Timmermans L, Godschalk RW, Theys J, Wouters BG, van Schooten FJ, et al. Diminished carcinogen detoxification is a novel mechanism for hypoxia-inducible factor 1-mediated genetic instability. J Biol Chem. 2010;285:14558–64, http://dx.doi.org/10.1074/jbc.M109.076323.